

## Spin pumping in d-wave superconductor/ferromagnet hybrids

S. J. Carreira<sup>1,\*</sup>, D. Sanchez-Manzano<sup>1,2</sup>, M.-W. Yoo<sup>1</sup>, K. Seurre<sup>1</sup>, V. Rouco<sup>1</sup>, A. Sander<sup>1</sup>, J. Santamaría<sup>2</sup>, A. Anane<sup>1</sup>, and J. E. Villegas<sup>1</sup>

<sup>1</sup>Unité Mixte de Physique, CNRS, Thales, Université Paris-Saclay, 91767, Palaiseau, France.

<sup>2</sup>Grupo de Física de Materiales Complejos (GFMC). Dpto. de Física de Materiales. Facultad de Ciencias Físicas, UCM, Plaza Ciencias, 1 28040, Madrid, Spain.

Spin-pumping across ferromagnet/superconductor (F/S) interfaces has attracted much attention lately. Yet the focus has been mainly on s-wave superconductors-based systems whereas (high-temperature) d-wave superconductors such as  $\text{YBa}_2\text{Cu}_3\text{O}_{7-d}$  (YBCO) have received scarce attention despite their fundamental and technological interest. Here we use wideband ferromagnetic resonance to study spin-pumping effects in bilayers that combine a soft metallic  $\text{Ni}_{80}\text{Fe}_{20}$  (Py) ferromagnet and YBCO. We evaluate the spin conductance in YBCO by analyzing the magnetization dynamics in Py. We find that the Gilbert damping exhibits a drastic drop as the heterostructures are cooled across the normal-superconducting transition and then, depending on the S/F interface morphology, either stays constant or shows a strong upturn. This unique behavior is explained considering quasiparticle density of states at the YBCO surface, and is a direct consequence of zero-gap nodes for particular directions in the momentum space. Besides showing the fingerprint of d-wave superconductivity in spin-pumping, our results demonstrate the potential of high-temperature superconductors for fine tuning of the magnetization dynamics in ferromagnets using k-space degrees of freedom of d-wave/F interfaces.

\*Corresponding author: [santiago.carreira@cnrs-thales.fr](mailto:santiago.carreira@cnrs-thales.fr)

## Introduction

Spin injection into superconductors constitutes a very active research topic within the nascent field of superconducting spintronics, aiming at expanding spintronic functionalities by exploiting the dissipationless electron transport and quantum coherence characteristic of superconductivity [1–5].

Theory and experiments have shown that spin currents can flow into s-wave superconductors carried by equal-spin triplet Cooper pairs [1,2,6–9] or by superconducting quasiparticles [10,11], whose lifetime can exceed those of spin-polarized electrons in the normal state [12–16]. Spin-polarized quasiparticles can be efficiently injected into the superconductor (S) using an adjacent ferromagnet (F) by applying across the S/F interface a bias voltage that exceeds the superconducting gap [10,17]. This mechanism has been extensively explored in transport experiments with spin valves [13,18–21]. Another mechanism for inducing a non-equilibrium spin accumulation in superconductors is spin-pumping [22] using the resonant excitation of the ferromagnet's magnetization [23,24] as source of pure spin current. In these ferromagnetic resonance (FMR) experiments, the superconductor's efficiency as a spin-sink is evaluated via spin hall effect [25] or microwave absorption measurements [8,25–28], by monitoring the evolution of the resonant peak's linewidth across the superconducting transition. The assumption is that the changes of the magnetic damping (which lead to a narrowing/broadening of the resonance linewidth [23,24]) reflect variations in the spin relaxation rate when the superconducting gap opens, because this alters both the spin transmission across the superconductor/ferromagnet interface and the relaxation mechanisms within the superconductor. Pioneering experiments performed on  $\text{Ni}_{80}\text{Fe}_{20}/\text{Nb}$  (Py/Nb) bilayers have found that the opening of the superconducting gap induces an abrupt FMR linewidth narrowing when temperature is swept across the superconducting transition [26]. This was explained by considering that the opening of the superconducting

gap leads to a vanishing density of states at the Fermi level, thereby hindering the transmission of spin polarized electrons across the interface. More recent work on GdN (F) / NbN (S) multilayers has found a different behavior, in which the Gilbert damping initially peaks across the superconducting transition, and diminishes below the normal-state value upon further temperature decrease [29]. That behavior was associated to the presence of spin-orbit scattering at the interface [30]. In contrast to the two examples above, studies carried out on Py/Nb multilayers with an adjacent strong spin-orbit coupling metal (Pt) found a steady broadening of the linewidth below  $T_C$ , which was interpreted in terms of enhanced spin transport across the superconductor due to the generation of equal-spin triplet superconductivity [7,8]. Adding a new piece to the puzzle, very recent theory shows that, if the superconducting gap is suppressed near S/F the interface, the presence of quasiparticle surface states can also produce an enhancement of spin transport into the superconductor below  $T_C$  [31]. The strikingly wide variety of observed behaviors illustrates the complexity of the underlying physics, the importance of the interfacial properties, and the fact that the conditions for predominance and interplay of the different proposed scenarios (quasiparticles and triplet superconductivity) is far from being fully understood. Beyond raising these fundamental questions, it is interesting that the experimental investigations have evidenced that superconductivity may be exploited for tuning magnetization dynamics.

The experiments discussed so far are based on conventional (low- $T_C$ ) s-wave superconductors, which present an isotropic superconducting gap. In contrast, in unconventional (high- $T_C$ ) d-wave ones the gap is suppressed along particular directions in the momentum space, and there exists a  $\pi$  superconducting-phase shift between d-wave lobes [32–34]. While spin diffusion effects in d-wave superconductors have been discussed in the context of electrical measurements [35–40], to our knowledge spin-pumping and the effects of the onset of superconducting pairing on the spin-sink behavior of d-wave cuprates

remain unexplored. Notice that, at variance to s-wave superconductors, the presence of zero-gap nodes may provide channels for injection of spin-polarized electrons, even in the superconducting state. Consequently, the effects of superconductivity on spin-pumping and magnetization dynamics are expectedly different in the case of s-wave superconductors. Here we experimentally investigate this issue using c-axis YBCO/Py heterostructures with different interface structure. In all cases, we observe an abrupt linewidth narrowing across the superconducting transition, similar to that observed in Py/Nb s-wave system [26], which suggests that, right below the critical temperature, the opening of the d-wave gap significantly suppress spin-pumping. However, upon further temperature decrease, the behavior of the linewidth depends on the YBCO surface morphology. For the smoother YBCO films, we observe no further evolution of the linewidth. However, in the presence of a faceted YBCO surfaces, the linewidth monotonically widens as the temperature is decreased below  $T_c$ . This behavior can be explained considering the interfacial density of quasiparticle states, which depends on the YBCO surface morphology due to the anisotropic character of d-wave superconductivity. These results thereby provide a fingerprint of d-wave superconductivity in the physics of spin-pumping. At the same time, they underline the need of a theoretical framework that specifically addresses the role of the mechanisms at play (quasiparticle density of states [41,42], changes in the spin-imbalance relaxation [43] and dynamic generation of triplet pairs [44,45]) in the context of d-wave superconductivity. Finally, this work demonstrates the potential of high-temperature superconductors for manipulating the magnetization dynamics of metallic ferromagnets, in a way that could be engineered by choosing the orientation of the d-wave/F interface.

## **Experimental**

We have studied different multilayers, namely c-axis  $\text{YBa}_2\text{Cu}_3\text{O}_7$  (30 nm)/ $\text{Ni}_{80}\text{Fe}_{20}$  (15 nm)/Al (3 nm) grown on (001)  $\text{SrTiO}_3$  and on (001)  $\text{NdGaO}_3$  – respectively referred to as

STO//S/F and NGO//S/F– and  $\text{YBa}_2\text{Cu}_3\text{O}_7$  (30 nm)/Au (5 nm)/ $\text{Ni}_{80}\text{Fe}_{20}$  (15 nm)/Al (3 nm) on STO –referred to as STO//S/Au/F. The YBCO films were grown by pulsed laser deposition (PLD) using an excimer laser ( $\lambda = 305$  nm) at a temperature of 700 °C and oxygen pressure of 0.36 mbar. Optimum oxygenation was ensured by raising the  $\text{O}_2$  pressure to 760 mbar during cooldown. Where applicable, the Au interlayer (aimed at preventing eventual redox reactions between YBCO and Py) was subsequently grown in-situ by PLD, at room temperature and in pure Ar atmosphere. Under this growth conditions, the onset of superconducting transition determined by resistivity measurements is typically around  $T_c \sim 85$  K, regardless of the substrate and presence of an Au overlayer. The structural properties of the as-grown YBCO films were studied by high-angle X-ray diffraction, which confirmed c-axis (001) epitaxial growth on both substrates STO and NGO, as well as the absence of parasitic phases. However, the YBCO’s surface morphology is very different depending of the substrate. As evidenced by the Atomic Force Microscopy (AFM) shown in Fig. 1, YBCO films on STO present a flat surface (rms roughness  $\sim 3$  nm), while YBCO on NGO presents a much rougher surface with a high density of  $\sim 15$  to 20 nm tall crystallites that result in a strongly faceted

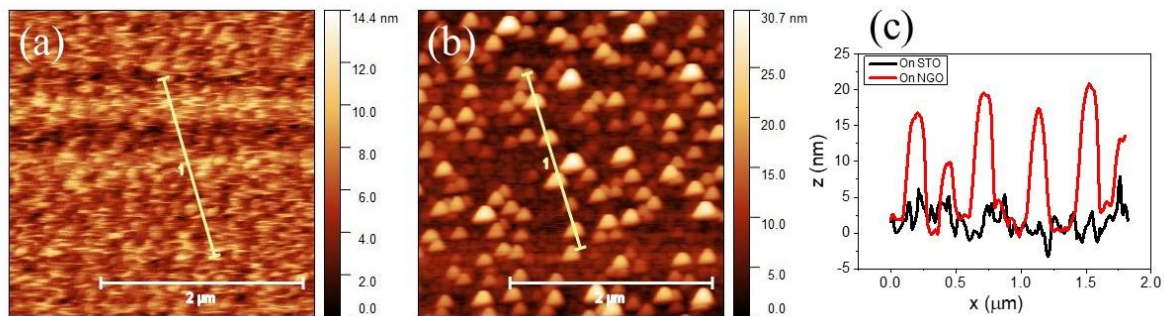


FIG. 1: AFM images measured on a  $3 \times 3 \mu\text{m}^2$  area of a YBCO thin film grown on (a) STO (001) and (b) NGO (001). The height profiles shown in (c) were measured along the lines indicated in (a) and (b) respectively.

surface.

The Py layer and Al capping (aimed at preventing Py surface oxidation) were subsequently deposited on the YBCO *ex-situ*, using rf-sputtering in pure Ar atmosphere at

room temperature, without breaking vacuum between each layer deposition. Control samples consisting of single Py films grown on both SrTiO<sub>3</sub> and NdGaO<sub>3</sub> (labeled as STO//F,

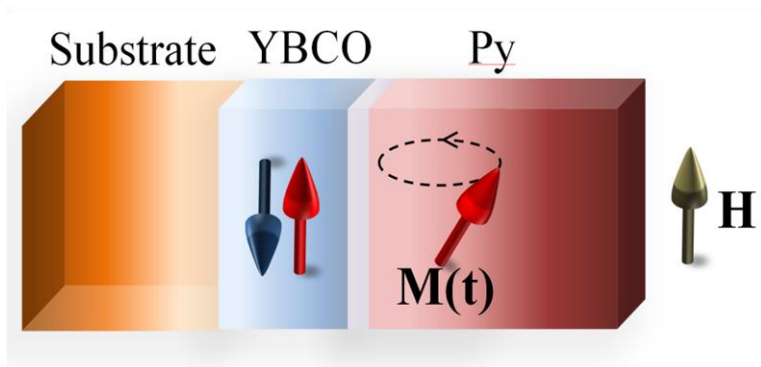


FIG. 2. Sketch of the multilayer structure and experimental geometry for the FMR experiments.

STO//Au/F and NGO//F) were studied. The samples' size is in all cases 5x5 mm<sup>2</sup>.

The experimental geometry considered for the FMR experiments is sketched in Fig. 2. A DC magnetic field  $H$  is applied parallel to the sample plane in order to saturate the magnetization of the Py and the excitation of the spin system is obtained with an RF magnetic field applied perpendicular to the DC field, using a coplanar waveguide. A DC field sweep is performed around the resonance field  $H_{res}$ , where the lorentzian dynamical susceptibility of the ferromagnetic layer peaks. A magnetic field modulation at low frequency (2 kHz) is used to measure the derivative of the absorbed power  $dP/dH$  with respect to the DC component of the magnetic field to improve the signal to noise ratio. When the Kittel resonant condition is fulfilled and neglecting the small magnetic anisotropy of Py, the resonant microwave frequency  $f$  and field  $H_{res}$  are related according to the Kittel formula [46],

$$f = \gamma\mu_0\sqrt{H_{res}(H_{res} + M_s)} \quad (\text{Eq. 1})$$

where  $\gamma$  is the gyromagnetic factor and  $M_s$  is the saturation magnetization. For each microwave frequency and temperature, the peak-to-peak linewidth  $\Delta H_{pp}$  and the resonance field  $H_{res}$  were

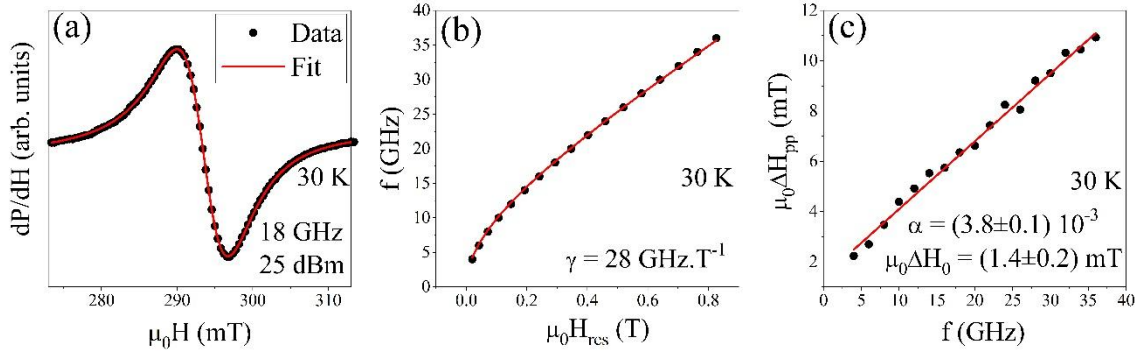


FIG. 3. Typical (a) FMR absorption spectrum and fit, (b)  $f$  vs  $H_{\text{res}}$  and (c)  $\Delta H_{\text{pp}}$  vs  $f$  obtained for the sample STO//S/Au/F at 30 K. The fits in (b) and (c) follows the FMR equations (1) and (2).

determined by fitting the FMR  $dP/dH$  absorption spectrum to the derivative of a Lorentzian function, as is shown in Fig. 3 (a). For all samples studied the linewidth is well described by the usual linear expression [24],

$$\Delta H_{\text{pp}} = \frac{2\alpha f}{\sqrt{3}\mu_0\gamma} + \Delta H_0 \quad (\text{Eq. 2})$$

where  $\Delta H_0$  is the frequency-independent contribution or inhomogeneous broadening and  $\alpha$  is the Gilbert damping factor. We explored the frequency range  $4 \text{ GHz} < f < 36 \text{ GHz}$  for all samples, allowing to plot the resonance field and linewidth as a function of the frequency, as respectively shown in Fig. 3 (b) and (c). The values of  $\alpha$  and  $\Delta H_0$  for each temperature are obtained from the fits, according to the equations (1) and (2), and their corresponding error bars are calculated from the linear regression of the fits.

## Results

Fig. 4 (a) shows an example of the temperature-dependent FMR linewidth at two particular RF frequencies (11 and 13 GHz), for a NGO//S/F bilayer (open symbols) and the NGO//F single film used as a control sample (closed symbols). The background behavior is qualitatively similar for both samples, and displays a steady linewidth broadening with decreasing temperature. This behavior has been observed in earlier FMR experiments on single Py thin films [47–50], where it was ascribed to the presence of magnetic oxides

(NiFeO<sub>x</sub>) with a typical order temperature in the range 10 K - 50 K, which would provide an extrinsic spin relaxation channel at low temperature [47–50]. Notice, however, that in the case of the superconducting sample, the low-temperature broadening is markedly enhanced with respect to the control sample.

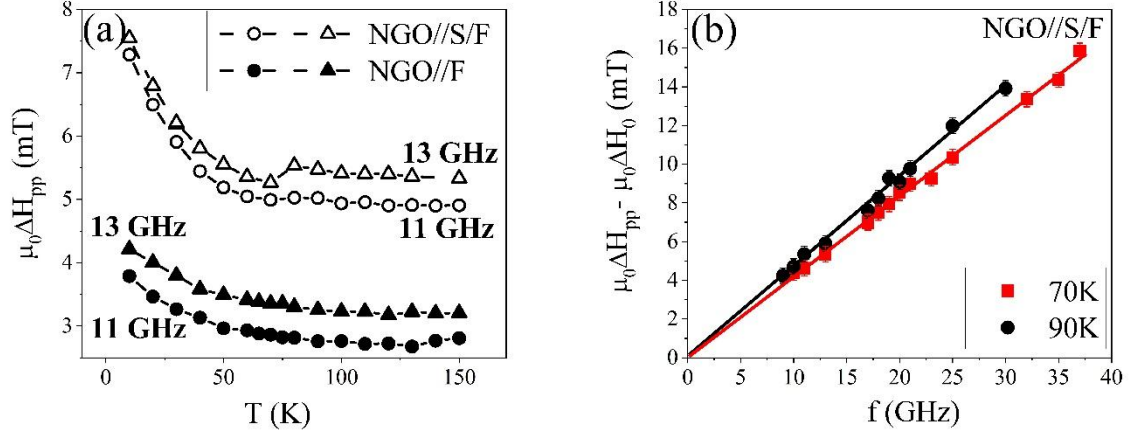
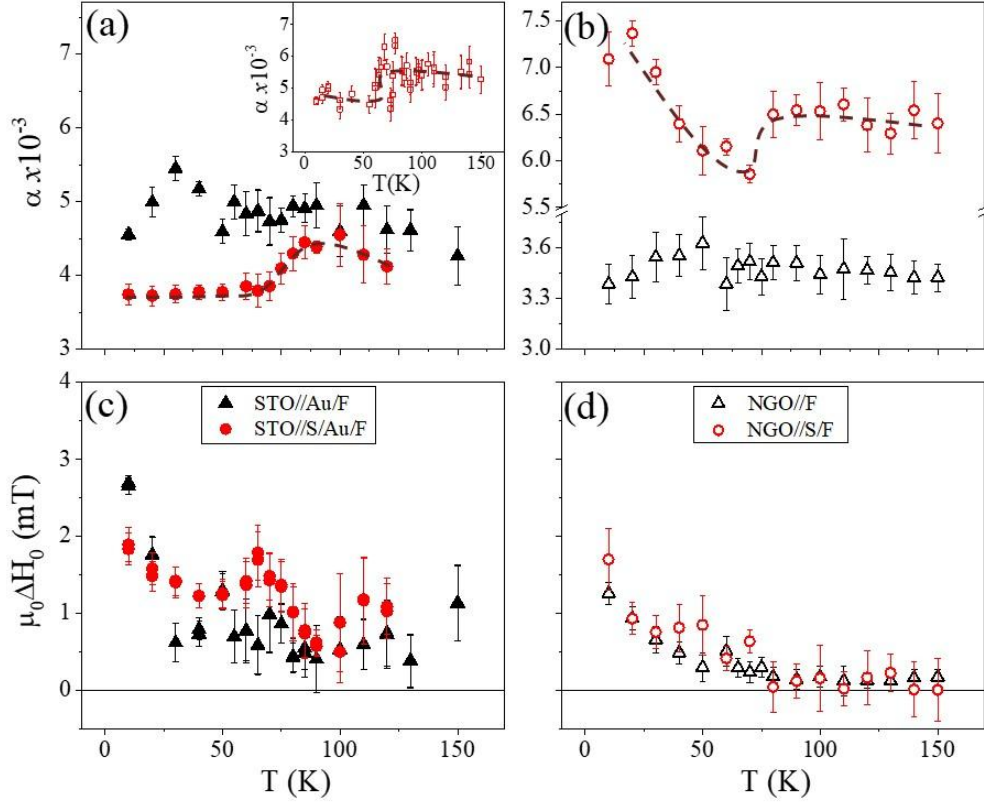


FIG. 4. (a) Temperature dependence of the FMR linewidth,  $\Delta H_{pp}$ , measured at (circles) 11 GHz and (triangles) 13 GHz for the samples NGO//S/F (open symbols) and NGO//F (triangles). The dash lines are guides to the eye. (b)  $\Delta H_{pp} - \Delta H_0$  vs  $f$  for the sample NGO//S/F obtained at temperatures just above and below the superconducting critical temperature of the YBCO. The straight lines correspond to linear fits of the data points.

Superposed to the background trend, the NGO//S/F bilayer shows another distinctive feature: a “kink” is observed at temperatures around  $T \sim 70 - 80$  K. This is clearer for  $f = 13$  GHz than for  $f = 11$  GHz. This “kink” corresponds to a drop of the damping factor  $\alpha$  across the superconducting transition, as evidenced in Fig. 4 (b). Here, the linewidth (after subtraction of the frequency-independent broadening  $\Delta H_0$ ) is plotted as a function of the frequency. In good agreement with Eq. 2, a linear relationship is observed. The slope of the straight line is proportional to the damping factor  $\alpha$ . Based on the linear behavior observed in  $\Delta H$  vs.  $f$  for a broadband frequency range, we consider that the 2-magnon scattering can be ruled out as a dominant relaxation mechanism of the magnetic system in our samples [51]. One can see that it is different above (90 K) and below (70 K) the superconducting transition of YBCO. From this graph it is also evident that broadband measurements are crucial to quantify the linewidth changes across the superconducting transition, and to univocally



ascribe them to a variation of the damping factor. The effect of the superconductor is striking on the temperature dependence of the damping coefficient  $\alpha(T)$ , which can be obtained together with the temperature dependent inhomogeneous broadening  $\Delta H_0(T)$  by applying the



analysis described above to a series of  $\Delta H_{PP}(f)$  measured at different temperatures.

FIG. 5. Temperature dependence of the [(a) and (b)] magnetic damping  $\alpha$  and [(c) and (d)] inhomogeneous broadening  $\Delta H_0$  for the samples STO//S/Au/F and STO//Au/F (closed symbols) and NGO//S/F and NGO//F (open symbols)). Data in circles corresponds to the samples with YBCO as a bottom layer and the control samples without YBCO are denoted with triangles. The inset in (a) shows  $\alpha$  vs  $T$  for the sample STO//S/F. The dash lines are guides to eye.

In Fig. 5 (a) we show  $\alpha(T)$  for superconducting multilayers STO//S/Au/F (red circles, main panel) and STO//S/F (inset), together with the data (black circles) for a single Py film (sample STO//Au/F) used as reference. One can see that, when Py is combined with the superconductor, and regardless of the presence of an Au interlayer,  $\alpha(T)$  drops by  $\sim 10$ - $15\%$  between 90 K and 70 K. Upon further temperature decrease  $\alpha$  stays nearly constant. That is,  $\alpha$  drops across the superconducting transition, and remains constant thereafter. This contrasts

with the behavior of the STO//Au/F sample used as reference (black dots), which shows no clear change of  $\alpha$  within the explored temperature range. Notice also that the damping level  $\alpha \sim 4.5 \cdot 10^{-3}$  in the temperature range in which the YBCO is in the normal state ( $T > 90$  K) is comparable for the superconducting (STO//S/Au/F) and reference (STO//Au/F) samples. Fig. 5 (c) shows that  $\Delta H_0(T)$  behaves very similarly in the superconducting and reference samples. This implies that the presence of the YBCO does not create additional magnetic inhomogeneities in Py, and unambiguously demonstrates that in the present experiments the changes observed in the FMR linewidth reflect a decrease of the Gilbert damping factor across the superconducting transition. This effect can also be observed in the NGO//S/F bilayer [see Fig. 5 (b)] for which  $\alpha(T)$  shows a  $\sim 10\%$  drop across the superconducting transition (red circles) not observed in the reference NGO//F sample (black circles). As was pointed out for the STO substrate, the inhomogeneous broadening is not affected by presence of the YBCO layer, see Fig. 5 (d). However, there are two main differences when comparing samples grown on STO and on NGO. First, note that for NGO//S/F [Fig. 5 (b)] in the normal-state ( $T > 90$  K), the damping level  $\alpha \sim 6.5 \cdot 10^{-3}$  is significantly higher than for the reference sample NGO//F [Fig. 5 (d)]. Second, for NGO//S/F [Fig. 5 (b)]  $\alpha(T)$  does not remain constant below the superconducting transition, but it shows instead a steady increase with decreasing temperature.

### **Discussion**

The central observation is that the magnetic damping  $\alpha$  of Py in YBCO/Py heterostructures drops across the YBCO superconducting transition and that, upon further temperature decrease,  $\alpha$  either stays constant or shows an upturn depending on the substrate (STO or NGO) on which the heterostructures are grown. The initial drop across the transition is reminiscent of that observed in earlier experiments with s-wave superconductors [26]. That behavior was explained based on the idea that, when the superconducting gap opens in the

electronic density of states [52], the absence of available states impedes the injection of electronic spin at the Fermi level. Such blocking effect strengthens as temperature is lowered, because this makes the superconducting gap widen and the quasiparticle population diminish [52]. While such effect is consistent with the behavior of  $\alpha(T)$  for heterostructures grown on STO, it cannot fully account for the behavior of the samples grown on NGO: these show an upturn of the damping factor, which at low temperature reaches values higher than those observed above  $T_c$  [Fig. 5 (b)]. While a similar enhancement of spin-pumping in the superconducting phase observed in S/F interfaces [7,8] in the presence of a heavy metal (Pt) layer was explained by the generation of equal-spin triplets, in the present experiments we have no arguments nor evidence to support such scenario. Instead, we have considered the situation recently studied theoretically [42], in which an enhancement of spin-pumping in the superconducting phase is predicted in the presence of a quasiparticle surface states (Andreev bound states) at the interface with the F. In Ref. [42] s-wave superconductors were considered, for which the emergence of Andreev bound states leads to a suppression of the superconducting gap near the interface due to inverse proximity effect. However, in the case of d-wave superconductors, quasiparticle (Andreev) surface bound states appear *intrinsically*, due to the existence of zero-gap nodes along particular k-space directions [53]. This allows for an understanding of the distinct behaviors of samples grown in STO and NGO, which constitute indeed the fingerprint of d-wave superconductivity in spin-pumping experiments.

Spin-pumping into the S depends on the surface density of quasiparticle states: the larger the density of states, the larger the spin injection efficiency. Extending to d-wave superconductors the full calculations of existing for s-wave ones [42] is out of the present work's scope. However, an understanding of our experiments is at reach by looking at the local density of states at a d-wave/normal metal interface of finite transparency. Following [54], the normalized local density of quasiparticle states at the interface is:

$$\rho_{S_0}/\rho_N(E) = \frac{1 - (\sigma_N - 1)^2 |\Gamma_+ \Gamma_-|^2}{|1 + (\sigma_N - 1) \Gamma_+ \Gamma_- \exp(i\phi_- - i\phi_+)|^2} \quad (\text{Eq. 3})$$

where  $\rho_N$  is the normal-state electron density of states,  $\sigma_N = \frac{1}{1+Z^2}$  with  $Z$  the barrier strength at the interface,  $\Gamma_{\pm} = \frac{E - \sqrt{E^2 - |\Delta_{\pm}|^2}}{|\Delta_{\pm}|}$  with  $E$  the quasiparticle energy with respect to the Fermi level, and  $\phi_+$  (respectively  $\phi_-$ ) is the effective phase of the anisotropic pair potential  $\Delta_+$  ( $\Delta_-$ ). Temperature effects in the quasiparticle population can be taken into account by considering the gap amplitude  $\Delta(T) = \Delta_0 \tanh(b \sqrt{\frac{T_C}{T} - 1})$  and by convoluting  $\rho_{S_0}/\rho_N(E)$  with the derivative of the Fermi-Dirac distribution  $f_{FD}(E, T)$  [55],

$$\rho_S/\rho_N(E, T) = \int \rho_{S_0}/\rho_N(E') \frac{\partial f_{FD}}{\partial E}(E - E', T) dE' \quad (\text{Eq. 4})$$

Calculations of  $\rho_S/\rho_N(E, T)$  for interfaces normal to the YBCO crystallographic directions (001) and (110) are shown in Fig. 6 (a) and (b) respectively, considering a moderate interface transparency given  $Z = 2.5$ . The different behavior in Fig. 6(a) and 6(b) results from the anisotropic nature of the density of states at the YBCO surface. For a (001) surface, we observe at low energies ( $E < \Delta$ ) that the opening of the superconducting gap leads to a fast reduction of the density of states upon decreasing temperature, similarly as in s-wave superconductors. On the contrary, for the (110) case [Fig 6 (b)] we observe the emergence of Andreev bound states around  $E = 0$ , whose population gradually increases upon decreasing temperature, leading to a peak in the density of states. In our experiments, the microwave energy  $\hbar f \ll \Delta$ , and thus the relevant quantity is the density of states near the Fermi level ( $E \sim 0$ ) [42]. This is shown in the upper inset of Fig. 6 (b) for the two cases (001) and (110).

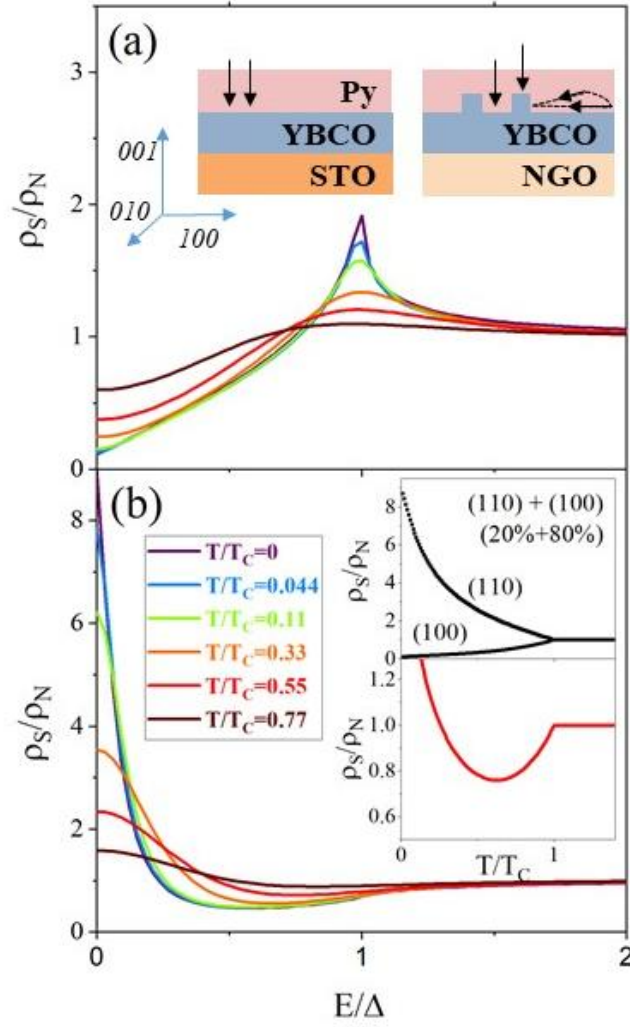


FIG. 6. Calculated density of states along the (a) (001) and (b) (110) crystallographic directions of the YBCO for different temperatures in the superconducting state. The sketches in (a) illustrate the possible directions for the spin injection according to their surface morphology, for the samples grown on STO and NGO. The upper inset in (b) displays the temperature dependence of the density of states along the (001) and (110) directions and the lower inset shows the resulting density of states when 20% / 80% contributions of the (001) and (110) are considered for the spin injection.

Based on the above, and considering the different topography of the samples on STO and on NGO, an understanding for the different  $\alpha(T)$  emerges. As sketched in the inset of Fig. 6 (a), in the case of STO the effects along (001) dominate, because of the smoother S/F interface. In this situation, the density of surface quasiparticle states is as in Fig. 6 (a) [56] and, as was observed for s-wave superconductors [26], we expect that  $\alpha(T)$  decays across the superconducting transition, in agreement with our experimental findings [Fig. 5 (a)]. For

samples grown on NGO, the faceted surface allows spin pumping into the YBCO basal (or *ab*) plane [sketch in the inset of Fig. 6 (a)]. This provides access to the large density of zero-energy quasiparticle states along (110). If we consider that the faceted morphology results in an effective density of states in which the contribution of directions presenting Andreev bound states weights 20% [lower inset in Fig 6 (b)], the calculated  $\rho_S/\rho_N(E, T)$  accounts for the behavior of  $\alpha(T)$  in the experiments [red in Fig. 5 (c)]: an abrupt drop across the transition, followed by an upturn upon further temperature decrease. Notice that a significant weight of the Andreev bound states in the density of states is reasonable for the samples grown on NGO, on the one hand, due to the large density of surface crystallites [Fig. 1 (b)] and on the other, due to the large electronic anisotropy of YBCO, whose conductivity in the basal (*ab*) plane is up to 10 times larger than along the c-axis [57–59]. Consistently, for the sample on NGO the damping is significantly higher than for the reference sample also in the normal-state (see Fig. 5 (b) for  $T > 90$  K), as Py contacts the YBCO not only on the c-axis surface but also on the more conducting basal (*ab*) plane. This results in a higher interfacial conductance than for the film grown on STO, which enhances the spin absorption and therefore the overall damping.

A final word concerning the impact of the Au interlayer. When the Au layer is deposited on YBCO, we observe no major effect on  $\alpha(T)$ , which indicates that its presence does not significantly change the interface transparency and is consistent with the fact the spin diffusion length of Au ( $\approx 50$  nm at 10 K) [60] is larger than the Au layer thickness. In the control (non-superconducting) samples, the presence of an Au interlayer between Py and the insulating substrate enhances the magnetic damping, which reflects that Au is a more efficient spin-sink than the substrate.

In summary, we have found that in d-wave superconductor/ferromagnet YBCO/Py multilayers, the opening of the superconducting gap reduces the spin-sinking efficiency and

results in a significant drop of the magnetic damping at the superconducting transition. However, upon further temperature decrease different behaviors are observed -either a plateau or an upturn- which correlates with the YBCO's surface morphology. This low-temperature upturn can be explained by the large density of quasiparticle surface bound states characteristic of d-wave superconductivity, which are accessible in faceted surfaces that directly expose the YBCO *ab* plane to the interface with the ferromagnet. This suggests that spin-pumping into quasiparticle bound states could be further enhanced by engineering the YBCO surface, for example by growing YBCO in different crystallographic directions, or by creating vicinal surfaces, to efficiently manipulate the magnetization dynamics in d-wave S/F hybrids. Finally, we hope that the present experiments will motivate further theoretical developments –for instance an extension of Ref. [31] to the case of d-wave superconductors– that may allow a more accurate quantitative analysis by including other ingredients, such as changes in the spin relaxation time in the superconducting state along different crystallographic directions [10,17].

### **Acknowledgements**

Work supported by ERC grant N° 647100 “SUSPINTRONICS”, French ANR grant ANR-15-CE24-0008-01 “SUPERTRONICS”, COST action “NanocoHybri” and EU H2020 Marie Curie Actions N° 890964 “SUPERMAGNONICS”.

### **References**

- [1] F. S. Bergeret, A. F. Volkov, and K. B. Efetov, *Long-Range Proximity Effects in Superconductor-Ferromagnet Structures*, Phys. Rev. Lett. **86**, 4096 (2001).
- [2] M. Eschrig, *Spin-Polarized Supercurrents for Spintronics*, Phys. Today **64**, 43 (2011).
- [3] M. G. Blamire and J. W. A. Robinson, *The Interface between Superconductivity and*

- Magnetism: Understanding and Device Prospects*, J. Phys. Condens. Matter **26**, 453201 (2014).
- [4] J. Linder and J. W. A. Robinson, *Superconducting Spintronics*, Nat. Phys. **11**, 307 (2015).
- [5] M. Eschrig, *Spin-Polarized Supercurrents for Spintronics: A Review of Current Progress*, Rep. Prog. Phys. **78**, 104501 (2015).
- [6] A. Kadigrobov, R. I. Shekhter, and M. Jonson, *Quantum Spin Fluctuations as a Source of Long-Range Proximity Effects in Diffusive Ferromagnet-Super Conductor Structures*, Eur. Lett. **54**, 394 (2001).
- [7] K.-R. Jeon, C. Ciccarelli, A. J. Ferguson, H. Kurebayashi, L. F. Cohen, X. Montiel, M. Eschrig, J. W. A. Robinson, and M. G. Blamire, *Enhanced Spin Pumping into Superconductors Provides Evidence for Superconducting Pure Spin Currents*, Nat. Mater. **17**, 499 (2018).
- [8] K.-R. Jeon, C. Ciccarelli, H. Kurebayashi, L. F. Cohen, X. Montiel, M. Eschrig, S. Komori, J. W. A. Robinson, and M. G. Blamire, *Exchange-Field Enhancement of Superconducting Spin Pumping*, Phys. Rev. B **99**, 024507 (2019).
- [9] F. S. Bergeret, A. F. Volkov, and K. B. Efetov, *Odd Triplet Superconductivity and Related Phenomena in Superconductor-Ferromagnet Structures*, Rev. Mod. Phys. **77**, 1321 (2005).
- [10] S. Takahashi, H. Imamura, and S. Maekawa, *Spin Imbalance and Magnetoresistance in Ferromagnet/Superconductor/Ferromagnet Double Tunnel Junctions*, Phys. Rev. Lett. **82**, 3911 (1999).
- [11] S. Takahashi and S. Maekawa, *Spin Injection and Detection in Magnetic Nanostructures*, Phys. Rev. B **67**, 052409 (2003).
- [12] N. Poli, J. P. Morten, M. Urech, A. Brataas, D. B. Haviland, and V. Korenivski, *Spin*



- Injection and Relaxation in a Mesoscopic Superconductor*, Phys. Rev. Lett. **100**, 136601 (2008).
- [13] H. Yang, S.-H. Yang, S. Takahashi, S. Maekawa, and S. S. P. Parkin, *Extremely Long Quasiparticle Spin Lifetimes in Superconducting Aluminium Using MgO Tunnel Spin Injectors*, Nat. Mater. **9**, 586 (2010).
- [14] H. L. Zhao and S. Hershfield, *Tunneling, Relaxation of Spin-Polarized Quasiparticles, and Spin-Charge Separation in Superconductors*, Phys. Rev. B **52**, 3632 (1995).
- [15] S. A. Kivelson and D. S. Rokhsar, *Bogoliubov Quasiparticles, Spinons, and Spin-Charge Decoupling in Superconductors*, Phys. Rev. B **41**, 11693(R) (1990).
- [16] C. H. L. Quay, D. Chevallier, C. Bena, and M. Aprili, *Spin Imbalance and Spin-Charge Separation in a Mesoscopic Superconductor*, Nat. Phys. **9**, 84 (2013).
- [17] M. Johnson, *Spin Coupled Resistance Observed in Ferromagnet-Superconductor-Ferromagnet Trilayers*, Appl. Phys. Lett. **65**, 1460 (1994).
- [18] A. K. Suzka, F. S. Bergeret, and A. Berger, *Domain-Wall-Induced Magnetoresistance in Pseudo-Spin-Valve/Superconductor Hybrid Structures*, Phys. Rev. B **85**, 24529 (2012).
- [19] T. Wakamura, N. Hasegawa, K. Ohnishi, Y. Niimi, and Y. Otani, *Spin Injection into a Superconductor with Strong Spin-Orbit Coupling*, Phys. Rev. Lett. **112**, 36602 (2014).
- [20] K. Ohnishi, Y. Ono, T. Nomura, and T. Kimura, *Significant Change of Spin Transport Property in Cu/Nb Bilayer Due to Superconducting Transition*, Sci. Rep. **4**, 6260 (2014).
- [21] J. Y. Gu, J. A. Caballero, R. D. Slater, R. Loloee, and W. P. Pratt, *Direct Measurement of Quasiparticle Evanescent Waves in a Dirty Superconductor*, Phys. Rev. B **66**, 140507(R) (2002).
- [22] S. Takahashi, *Physical Principles of Spin Pumping BT - Handbook of Spintronics*, in

- edited by Y. Xu, D. D. Awschalom, and J. Nitta (Springer Netherlands, Dordrecht, 2016), pp. 1445–1480.
- [23] E. Landau, Lev Davidovich Lifshitz, *On the Theory of the Dispersion of Magnetic Permeability in Ferromagnetic Bodies*, Phys. Z. Sowjet. **8**, 153 (1935).
- [24] T. L. Gilbert, *A Phenomenological Theory of Damping in Ferromagnetic Materials*, IEEE Trans. Magn. **40**, 3443 (2004).
- [25] K.-R. Jeon, C. Ciccarelli, H. Kurebayashi, J. Wunderlich, L. F. Cohen, S. Komori, J. W. A. Robinson, and M. G. Blamire, *Spin-Pumping-Induced Inverse Spin Hall Effect in Nb/Ni<sub>80</sub>Fe<sub>20</sub> Bilayers and Its Strong Decay Across the Superconducting Transition Temperature*, Phys. Rev. Appl. **10**, 014029 (2018).
- [26] C. Bell, S. Milikisyants, M. Huber, and J. Aarts, *Spin Dynamics in a Superconductor-Ferromagnet Proximity System*, Phys. Rev. Lett. **100**, 47002 (2008).
- [27] K.-R. Jeon, C. Ciccarelli, H. Kurebayashi, L. F. Cohen, S. Komori, J. W. A. Robinson, and M. G. Blamire, *Abrikosov Vortex Nucleation and Its Detrimental Effect on Superconducting Spin Pumping in Pt/Nb/Ni<sub>80</sub>Fe<sub>20</sub>/Nb/Pt Proximity Structures*, Phys. Rev. B **99**, 144503 (2019).
- [28] K.-R. Jeon, C. Ciccarelli, H. Kurebayashi, L. F. Cohen, X. Montiel, M. Eschrig, T. Wagner, S. Komori, A. Srivastava, J. W. A. Robinson, and M. G. Blamire, *Effect of Meissner Screening and Trapped Magnetic Flux on Magnetization Dynamics in Thick Nb/Ni<sub>80</sub>Fe<sub>20</sub>/Nb Trilayers*, Phys. Rev. Appl. **11**, 014061 (2019).
- [29] Y. Yao, Q. Song, Y. Takamura, J. P. Cascales, W. Yuan, Y. Ma, Y. Yun, X. C. Xie, J. S. Moodera, and W. Han, *Probe of Spin Dynamics in Superconducting NbN Thin Films via Spin Pumping*, Phys. Rev. B **97**, 224414 (2018).
- [30] M. Inoue, M. Ichioka, and H. Adachi, *Spin Pumping into Superconductors: A New Probe of Spin Dynamics in a Superconducting Thin Film*, Phys. Rev. B **96**, 24414

- (2017).
- [31] M. A. Silaev, *Large Enhancement of Spin Pumping Due to the Surface Bound States in Normal Metal/Superconductor Structures*, (2020).
- [32] Z.-X. Shen, D. S. Dessau, B. O. Wells, D. M. King, W. E. Spicer, A. J. Arko, D. Marshall, L. W. Lombardo, A. Kapitulnik, P. Dickinson, S. Doniach, J. DiCarlo, T. Loeser, and C. H. Park, *Anomalously Large Gap Anisotropy in the A-b Plane of  $\text{Bi}_2\text{Sr}_2\text{CaCu}_2\text{O}_{8+\delta}$* , Phys. Rev. Lett. **70**, 1553 (1993).
- [33] H. Aubin, K. Behnia, M. Ribault, R. Gagnon, and L. Taillefer, *Angular Position of Nodes in the Superconducting Gap of YBCO*, Phys. Rev. Lett. **78**, 2624 (1997).
- [34] J. R. Kirtley, C. C. Tsuei, Ariando, C. J. M. Verwijs, S. Harkema, and H. Hilgenkamp, *Angle-Resolved Phase-Sensitive Determination of the in-Plane Gap Symmetry in  $\text{YBa}_2\text{Cu}_3\text{O}_{7-\delta}$* , Nat. Phys. **2**, 190 (2006).
- [35] V. Peña, Z. Sefrioui, D. Arias, C. Leon, J. Santamaria, J. L. Martinez, S. G. E. te Velthuis, and A. Hoffmann, *Giant Magnetoresistance in Ferromagnet/Superconductor Superlattices*, Phys. Rev. Lett. **94**, 57002 (2005).
- [36] C. Visani, Z. Sefrioui, J. Tornos, C. Leon, J. Briatico, M. Bibes, a. Barthélémy, J. Santamaría, and J. E. Villegas, *Equal-Spin Andreev Reflection and Long-Range Coherent Transport in High-Temperature Superconductor/Half-Metallic Ferromagnet Junctions*, Nat. Phys. **8**, 539 (2012).
- [37] Z. Sefrioui, D. Arias, V. Peña, J. E. Villegas, M. Varela, P. Prieto, C. León, J. L. Martinez, and J. Santamaria, *Ferromagnetic/Superconducting Proximity Effect in  $\text{La}_{0.7}\text{Ca}_{0.3}\text{MnO}_3/\text{YBa}_2\text{Cu}_3\text{O}_{7-\delta}$  Superlattices*, Phys. Rev. B **67**, 214511 (2003).
- [38] Z. P. Niu and D. Y. Xing, *Spin-Triplet Pairing States in Ferromagnet/Ferromagnet/d-Wave Superconductor Heterojunctions with Noncollinear Magnetizations*, Phys. Rev. Lett. **98**, 57005 (2007).

- [39] S. Soltan, J. Albrecht, and H.-U. Habermeier, *Ferromagnetic/Superconducting Bilayer Structure: A Model System for Spin Diffusion Length Estimation*, Phys. Rev. B **70**, 144517 (2004).
- [40] N.-C. Yeh, R. P. Vasquez, C. C. Fu, A. V. Samoilov, Y. Li, and K. Vakili, *Nonequilibrium Superconductivity under Spin-Polarized Quasiparticle Currents in Perovskite Ferromagnet-Insulator-Superconductor Heterostructures*, Phys. Rev. B **60**, 10522 (1999).
- [41] T. T. Heikkilä, M. Silaev, P. Virtanen, and F. S. Bergeret, *Thermal, Electric and Spin Transport in Superconductor/Ferromagnetic-Insulator Structures*, Prog. Surf. Sci. **94**, 100540 (2019).
- [42] M. A. Silaev, *Large Enhancement of Spin Pumping Due to the Surface Bound States in Normal Metal/Superconductor Structures*, Phys. Rev. B **102**, 180502 (2020).
- [43] F. S. Bergeret, M. Silaev, P. Virtanen, and T. T. Heikkilä, *Colloquium: Nonequilibrium Effects in Superconductors with a Spin-Splitting Field*, Rev. Mod. Phys. **90**, 41001 (2018).
- [44] M. Houzet, *Ferromagnetic Josephson Junction with Precessing Magnetization*, Phys. Rev. Lett. **101**, 57009 (2008).
- [45] T. Yokoyama and Y. Tserkovnyak, *Tuning Odd Triplet Superconductivity by Spin Pumping*, Phys. Rev. B **80**, 104416 (2009).
- [46] C. Kittel, *On the Theory of Ferromagnetic Resonance Absorption*, Phys. Rev. **73**, 155 (1948).
- [47] S. Mizukami, Y. Ando, and T. Miyazaki, *Effect of Spin Diffusion on Gilbert Damping for a Very Thin Permalloy Layer in Cu/Permalloy/Cu/Pt Films*, Phys. Rev. B **66**, 104413 (2002).
- [48] L. Frangou, G. Forestier, S. Auffret, S. Gambarelli, and V. Baltz, *Relaxation*

- Mechanism in NiFe Thin Films Driven by Spin Angular Momentum Absorption throughout the Antiferromagnetic Phase Transition in Native Surface Oxides*, Phys. Rev. B **95**, 54416 (2017).
- [49] O. Gladii, L. Frangou, G. Forestier, R. L. Seeger, S. Auffret, I. Joumard, M. Rubio-Roy, S. Gambarelli, and V. Baltz, *Unraveling the Influence of Electronic and Magnonic Spin-Current Injection near the Magnetic Ordering Transition of IrMn Metallic Antiferromagnets*, Phys. Rev. B **98**, 94422 (2018).
- [50] Y. Zhao, Q. Song, S.-H. Yang, T. Su, W. Yuan, S. S. P. Parkin, J. Shi, and W. Han, *Experimental Investigation of Temperature-Dependent Gilbert Damping in Permalloy Thin Films*, Sci. Rep. **6**, 22890 (2016).
- [51] W. K. Peria, T. A. Peterson, A. P. McFadden, T. Qu, C. Liu, C. J. Palmstrøm, and P. A. Crowell, *Interplay of Large Two-Magnon Ferromagnetic Resonance Linewidths and Low Gilbert Damping in Heusler Thin Films*, Phys. Rev. B **101**, 134430 (2020).
- [52] M. Tinkham, *Introduction to Superconductivity / Michael Tinkham* (McGraw-Hill, New York, 1975).
- [53] S. Kashiwaya and Y. Tanaka, *Tunnelling Effects on Surface Bound States in Unconventional Superconductors*, Reports Prog. Phys. **63**, 1641 (2000).
- [54] Y. Tanaka and S. Kashiwaya, *Local Density of States of Quasiparticles near the Interface of Nonuniform D-Wave Superconductors.*, Phys. Rev. B. Condens. Matter **53**, 9371 (1996).
- [55] W. K. Park, L. H. Greene, J. L. Sarrao, and J. D. Thompson, *Andreev Reflection at the Normal–metal/Heavy–fermion Superconductor  $\text{CeCoIn}_5$  Interface*, Vol. 72 (American Physical Society, n.d.).
- [56] J. Y. T. Wei, N. C. Yeh, D. F. Garrigus, and M. Strasik, *Directional Tunneling and*

*Andreev Reflection on YBa<sub>2</sub>Cu<sub>3</sub>O<sub>7</sub> –  $\delta$  Single Crystals: Predominance of d-Wave Pairing Symmetry Verified with the Generalized Blonder, Tinkham, and Klapwijk Theory*, Phys. Rev. Lett. **81**, 2542 (1998).

- [57] M. Tinkham, *Introduction to Superconductivity* (2004).
- [58] P. H. Kes, J. Aarts, V. M. Vinokur, and C. J. van der Beek, *Dissipation in Highly Anisotropic Superconductors*, Phys. Rev. Lett. **64**, 1063 (1990).
- [59] G. Blatter, V. B. Geshkenbein, and A. I. Larkin, *From Isotropic to Anisotropic Superconductors: A Scaling Approach*, Phys. Rev. Lett. **68**, 875 (1992).
- [60] M. Isasa, E. Villamor, L. E. Hueso, M. Gradhand, and F. Casanova, *Temperature Dependence of Spin Diffusion Length and Spin Hall Angle in Au and Pt*, Phys. Rev. B **91**, 24402 (2015).